POLITECNICO DI TORINO
Repository ISTITUZIONALE

Ga+ Ion Irradiation-Induced Tuning of Artificial Pinning Sites to Control Domain Wall Motion

(Article begins on next page)

25 April 2024

Article

Ga⁺ Ion Irradiation-Induced Tuning of Artificial Pinning Sites to Control Domain Wall Motion

Domenico Giuliano, Luca Gnoli, Valentin Ahrens, Massimo Ruo Roch, Markus Becherer, Giovanna Turvani, Marco Vacca, and Fabrizio Riente*

Cite This: ACS Appl. Electron. Mater. 2023, 5, 985−993

Read Online

ACCESS | 📊 Metrics & More | 📰 Article Recommendations

ABSTRACT: Domain-wall-based devices are considered one of the candidates for the next generation of storage memories and nanomagnetic logic devices due to their unique properties, such as nonvolatility, scalability, and low power consumption. Field or current-driven domain walls require a regular and controlled motion along the track in which they are stored in order to maintain the information integrity during operation. However, their dynamics can vary along the track due to film inhomogeneities, roughness of the edges, and thermal fluctuations. Consequently, the final position of the domain walls may be difficult to predict, making difficult the development of memory and logic applications. In this paper, we demonstrate how Ga⁺ ion irradiation can be used to locally modify the material properties of the Ta/CoFeB/MgO thin film, creating regions in which the domain wall can be trapped, namely motion barriers. The aim is to push the domain wall to overcome thin-film inhomogeneities effects, while stopping its motion at artificially defined positions corresponding to the irradiated regions. Increasing the driving force strength, the domain wall can escape, allowing the shifting between consecutive irradiated regions. In this way, the correct positioning of the domain walls after the motion is ensured. The study shows that the driving force strength, namely current density or magnetic field amplitude, needed to overcome the irradiated regions depends on the ion dose. These results show a reliable approach for domain wall manipulation, enabling a precise control of the domain wall position along a track with synchronous motion.

KEYWORDS: spintronics, perpendicular anisotropy, magnetic devices, racetrack memory, Ga⁺ irradiation, pinning, domain wall
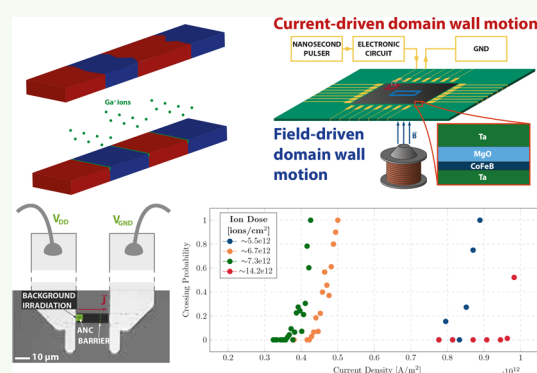
INTRODUCTION

Among different spintronic applications, domain-wall-based devices are considered one of the emerging candidates in the field of beyond-CMOS technologies.[1] Devices based on the motion of domain walls allow the implementation of new memory device concepts as well as the possibility to perform logic operations.[1−4] Relying on the spin of the electrons rather than their electrical charge, domain-wall-based devices show unique properties, such as nonphysical separation of bits, low power dissipation, and nonvolatility,[5−7] which attracted intense research during the past decades. In this scenario, ferromagnets sandwiched between an oxide and a heavy metal, such as Ta/CoFeB/MgO, play a fundamental role. They are characterized by perpendicular magnetic anisotropy (PMA), meaning that the magnetization of domains, in which the information is encoded, points toward the direction perpendicular to the film surface and also shows low depinning fields for domain wall motion.[8] Moreover, domain walls can be manipulated efficiently by spin−orbit torques (SOTs)[9,10] induced by the injection of a current into the heavy metal layer (e.g., Ta). As the current flows in it, a perpendicular spin-polarized current is

created due to spin Hall effect (SHE).[9,11,12] The electric control of the magnetization is a key aspect for the integration of single magnetic devices in more complex architectures.

Even though domain walls can be easily moved in such thin films, they are still strongly affected by the presence of defects during their motion.[13] Material defects are intrinsically created during the deposition of thin films due to formation of grains or due to the roughness introduced during the structuring process (i.e., lithography and etching). It means that the magnetic parameters are subjected to local variations, which are translated in domain wall motion pinning events. These pinning events can slow down or even stop the motion of domain walls. Moreover, such defects are randomly distributed, causing a not reliable domain wall motion, which is
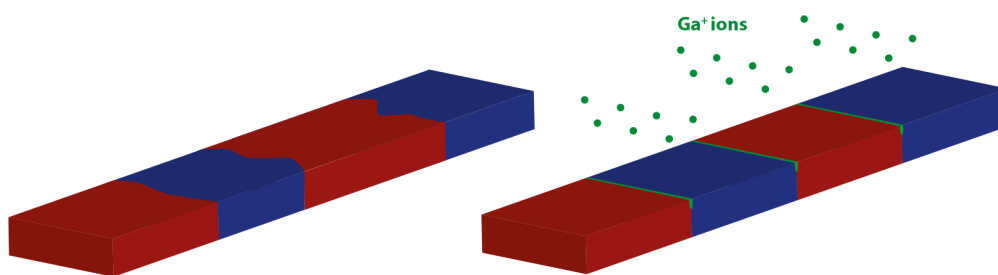
Figure 1. Schematic representation of the Ga$^+$ irradiation-induced creation of pinning sites. Pristine track on the left, where the domain size is not uniform due to thin-film inhomogeneities. Track with irradiated regions on the right. Here the domain walls are trapped at the green regions, corresponding to the irradiated ones. By designing the irradiation pattern, the domain walls positions can be defined and the domain size results uniform along the track.

required in real applications. One possible solution to account for this limitation is to push the domain walls with enough strength, whether augmenting the current or the magnetic field, to increase the probability to overcome the pinning sites. However, especially when considering multiple domain walls in a track, the motion can still be affected, causing variations of the spacing between consecutive domain walls, directly affecting the number of domains that can be hosted in a single track and making difficult the development of domain-wall-based applications.

In this work, we propose an approach to selectively stop the motion of domain walls by creating artificial pinning sites. They are regions in which the material parameters are intentionally modified to create motion barriers, namely artificial pinning sites. They have different strengths with respect to natural pinning spots, defined by defects. By tuning the strength of the pinning sites during the fabrication process, it is possible to stop domain walls in designed positions along the track (as shown in Figure 1), while still allowing the domain wall motion between these regions. The domain walls can still be moved selectively out of these designated rest positions by means of an external stimulus. According to this idea, a reliable shifting of the information can be achieved along the track. In order to create the artificial pinning sites, we exploit Ga$^+$ focused ion beam (FIB) irradiation. Studies on CoFeB/MgO already confirmed the possibility to tune the energy landscape, together with the magnetic parameters of the material, by irradiating the thin-film stack with He$^+$ ions[14,15] or with heavier ions such as Ga$^+$.[16−19] In a previous work on the Ta/CoFeB/MgO trilayer,[20] it was shown that K_{eff} can be increased up to a peak value by Ga$^+$ irradiation and then decreased for higher ion doses. Differently, lighter ions, such as He$^+$, when traversing the material lead to other modifications of the magnetic properties, resulting in a monotonic reduction of the effective magnetic anisotropy as the ion dose increases.[21] In the next sections, it will be shown how this nonmonotonic behavior allows obtaining confinements with tunable strength in a wide range of doses.

While Pt/Co/Pt studies showed how domain wall pinning can be used to create memory devices,[22−24] in our experiments we want to exploit the tuning of the magnetic properties of Ta/CoFeB/MgO by FIB Ga$^+$ irradiation to create and tune artificial motion barriers. The usage of heavier ions has been already demonstrated to be able to modify the energy landscape to create artificial nucleation centers (ANCs) to control the domain wall nucleation.[20] Here we exploit the Ga$^+$ ions irradiation onto ferromagnetic wires, patterned from Ta/CoFeB/MgO thin-film stack, to tailor the crossing of domain

walls through irradiated regions, defined as thin irradiation lines perpendicular to the track. The study is performed considering both field and current-driven domain wall motion, and it is supported by micromagnetic simulations to better understand the experimental results.

■ METHODS

The work is based on the Ta/Co$_{20}$Fe$_{60}$B$_{20}$/MgO trilayer. The layers composing the thin-film stack are Ta$_2$/CoFeB$_{1.1}$/MgO$_2$/Ta$_3$, where the subscripts express the nominal thickness in nanometers. The layers were deposited via confocal RF-magnetron sputtering, with a base pressure below 2×10^{-7} mbar. Each layer was deposited with 0.5 W/cm^2 of target power density, at a constant working pressure of 4 μbar, except for MgO, for which the pressure was kept at 1 μbar.

In order to increase the effective magnetic anisotropy, the sample was subjected to thermal annealing in a N$_2$ atmosphere at 275 °C for 5 min. The stack was patterned via UV optical lithography using AZECI3027 positive photoresist to create tracks and test structures. The structures were obtained by Ar$^+$ ion-beam etching. The last step involves the creation of the electrical contacts by depositing metal wires at the edges the patterned tracks. For this purpose, UV optical lithography was used to set up a lift-off mask. A metal stack consisting of a 5 nm of Ti adhesive layer, a 400 nm of Cu as conductive layer, and 50 nm of Cr for wire bonding was deposited by means of physical vapor deposition. After the lift-off process, wire bonding was used to connect the wire electrical contacts to the electronic circuit. The tracks and the test structures were irradiated via Ga$^+$ ion-based focused ion beam (Micrion 9500ex) with 50 keV in the range of 1×10^{12} to 4×10^{13} ions/cm^2.

The ferromagnetic structures were characterized using polar wide-field magneto-optical Kerr effect (WMOKE) microscopy. The measurements of the field-driven domain-wall motion were performed using millisecond long magnetic field pulses with an amplitude ranging from 0.5 to 2 mT. Here, a 6 μm wide ferromagnetic track was used. For current-driven domain-wall motion, the ferromagnetic tracks have a length above 15 μm and a lateral width of 5 μm, except for the track irradiated with an ion dose of 7.3×10^{12} ions/cm^2, where a track 7.5 μm wide was used. The current pulses were generated by an Agilent 81111A pulse generator in order to access pulse widths in the nanosecond range. The pulse generator was connected to a custom-design chip carrier to ensure the impedance matching and allowing for higher amplitude current density pulses in the range of 1×10^{11} to 1×10^{12} A/m^2. In both type of measurements, a WMOKE image was recorded after each pulse. The images were post processed by subtracting each of them with a reference image with initial magnetization state, resulting in a series of differential images with higher contrast, illustrating the motion of the domain wall during the measurement.

Lastly, micromagnetic simulations were performed using MuMax3.[25] The material parameters used in this work are listed in Table 1.[26] The values of the saturation magnetization M_S and of the uniaxial anisotropy K_u are chosen according to the experimental measurements presented in ref 20. The range of SOT current density

Table 1. Material Parameters Used in Micromagnetic Simulations

symbol	quantity	value
M_S	saturation magnetization	8.31×10^5 A/m
K_u	uniaxial anisotropy	5.58×10^5 J/m^3
D	Dzyaloshinskii–Moriya interaction constant	1×10^{-3} J/m^2
A	exchange stiffness	2×10^{-11} J/m^2
α	Gilbert damping constant	0.015
χ_{SOT}	SOT efficiency	-2
θ_{SHE}	spin Hall angle	0.15

used in the simulations goes from 1.5×10^{11} to 4.5×10^{11} A/m^2; the damping-like and the field-like parameters were calculated respectively as $a_j = \frac{\hbar}{2M_S e} \frac{\theta_{SHE}}{t}$ and $b_j = a_j \chi_{SOT}$. The simulation geometry consists of a microtrack of 512×1024 nm^2 and $t = 1$ nm in thickness. Even though the last parameter does not match the experimental one (which is 1.1 nm), the choice is justified considering that a change in the thickness of the thin-film produces a shifting to the absolute value anisotropy, while our focus is on the trend that its variation produces. The mesh grid size adopted in simulations is $1 \times 1 \times 1$ nm^3, and no periodic boundary conditions are used (this choice is discussed in the Micromagnetic Simulations section).

■ RESULTS AND DISCUSSION

Focused ion beam irradiation can locally modify the material parameters, such as the saturation magnetization and the anisotropy constant, which contribute to the effective anisotropy K_{eff} in the irradiated regions. Previous studies[14,15,27] show that during irradiation the interfaces are affected: for low ion doses, the CoFeB/MgO interface rearranges, producing an increase of the magnetic anisotropy. Increasing the ion dose, the irradiation produces an intermixing of the interface causing a decreasing of the saturation magnetization and of the effective magnetic anisotropy.[14] Moreover, also at the Ta/CoFeB interface an intermixing is produced, causing a broadening of the interface. Because of that, other parameters

(e.g., the DMI or the damping) are affected[27,28] as well. However, the changes in these parameters are not addressed in this study.

As shown in previous studies,[20] Ga$^+$ ions irradiation on the trilayer Ta/CoFeB/MgO produces an increase of the thin film effective anisotropy. Moreover, the influence of the irradiation can be observed in a variation of the average domain size and the coercivity. Similar effects on CoFeB/MgO films are reported using He$^+$ ions irradiation.[14,15,27] In particular, in ref 20 the domains become larger for low and medium Ga$^+$ ion dose up to a threshold found at $\approx 3.5 \times 10^{13}$ ions/cm^2. Thereafter, the average domain size gets smaller, dropping eventually to dimensions below the optical resolution for larger irradiation doses. Overall, the coercivity follows the same trend, reaching the zero value for high ion doses,[20] which may lead to the assumption that the thin film turned in-plane. The magnetic parameters were also measured around the average domain size peak with SQUID and VSM-magnetometer measurements, and an increase in the effective magnetic anisotropy was recorded. The behavior can be traced back into the expression of the effective magnetic anisotropy $K_{eff} = K_u - \frac{1}{2}\mu_0 M_S^2$, in which the quadratic dependence causes a higher influence of M_S over K_u. Therefore, we expect that for low and medium ion irradiation doses the reduction of the saturation magnetization has a major impact on the final value of the effective magnetic anisotropy.

The mentioned effects on the magnetic parameters can be used to locally tailor the magnetic properties of the material to create: (i) artificial nucleation centers (ANC)[20] to have a control over the nucleation position of the domain wall and (ii) to introduce pinning sites, namely motion barriers, able to confine the domain walls in a defined portion of the track.

In order to achieve that, an irradiation study is first needed to find the ion dose required for the creation of the ANC. Second, once the nucleation positions are defined, the outcomes of the irradiation study are used to find the range
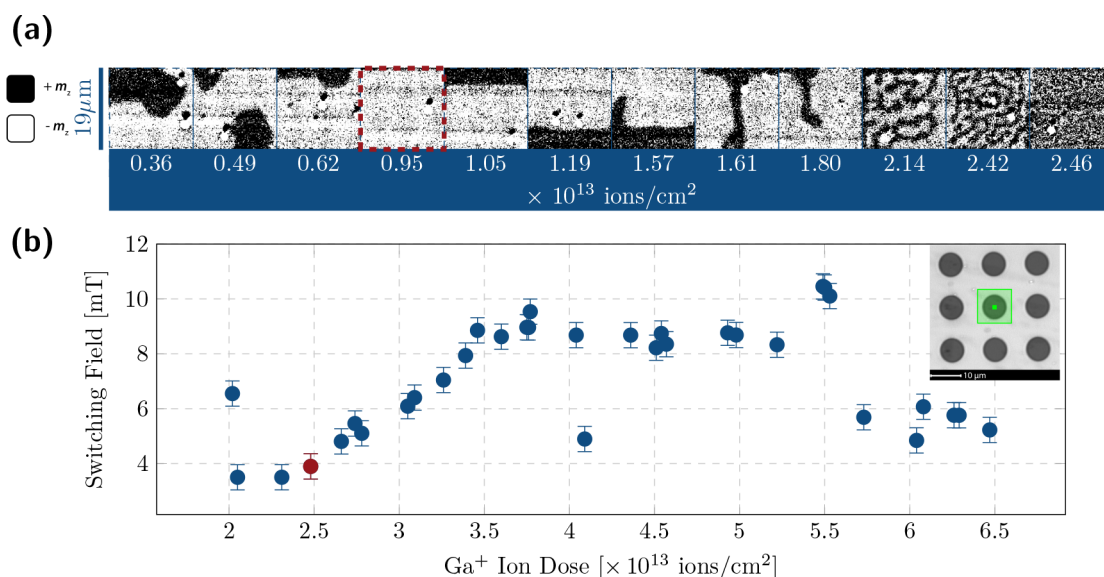

Figure 2. FIB irradiation study of the Ta/CoFeB/MgO/Ta stack. (a) Series of domain images in the zero-field state after irradiation at different ion doses ranging from 0.36×10^{13} to 2.46×10^{13} ions/cm^2. The red dashed square indicates the ion dose used for the background irradiation. (b) Evolution of the switching field of patterned microdisks after background plus ANC irradiation. The red point corresponds to the ion dose used for the artificial nucleation center irradiation. On the top right of the graph, a microscopic image of the structured microdisks used is shown. The green semitransparent square corresponds to the background irradiation, while the filled square corresponds to the ANC irradiation.
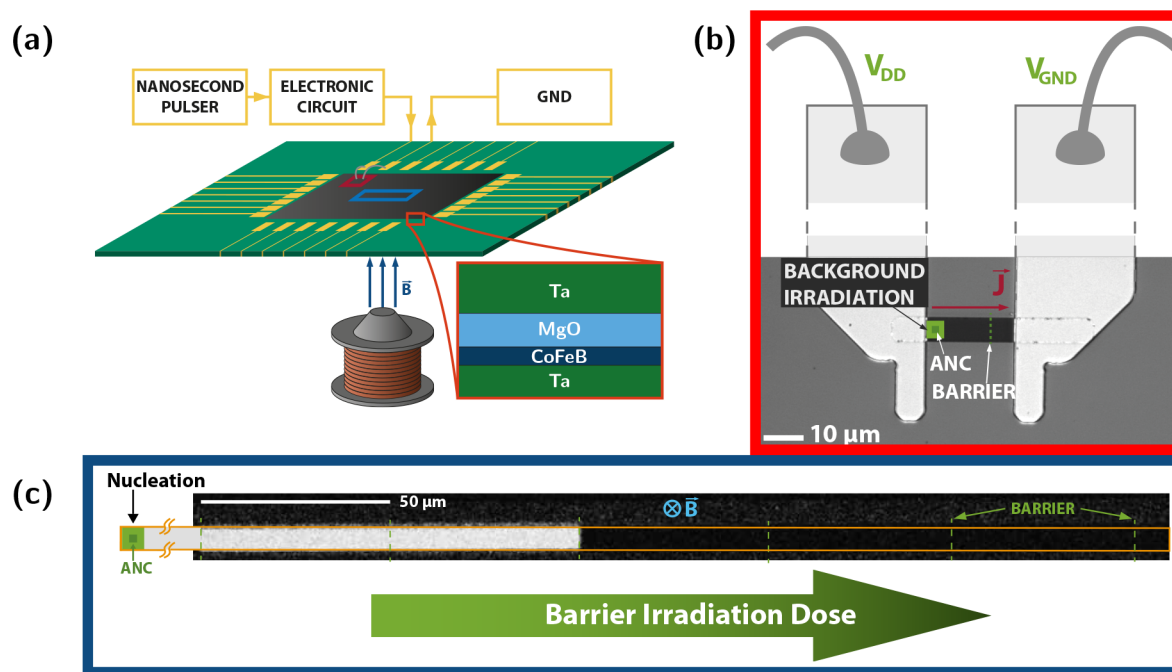
Figure 3. General layout of the experimental setup used to study the current and field-driven motion of magnetic domains across Ga$^+$ FIB irradiated barriers. (a) Scheme of the custom-designed chip carrier used for both the experiments. The sample (whose composition is illustrated in the zoomed image) is subjected to an external perpendicular magnetic field by means of an electromagnet underneath. A current pulse, generated from a nanosecond pulser, is injected into the sample thanks to wire bonding. An electronic circuit after the pulser ensures the impedance matching. (b) Microscopic image of a ferromagnetic track patterned into the sample. Cu/Cr contacts are deposited to allow the current flowing from the bonding wires to the magnetic track. The voltages defining the current direction are shown. (c) WMOKE image of a long track used to study the field-driven domain motion across the barriers.

of the ion doses that can be used to create the barriers, which represent the main scope of the present work. Different confinements with different ion doses are finally tested, with both field- and current-driven domain wall motion. At the end, the results are compared with the results from micromagnetic simulations.

Irradiation Study. In this study, Ga$^+$ ion irradiation is employed to locally reduce the switching field in a designated region and to provide a reliable mean of nucleation for domains on magnetic tracks. Recalling previous experiments,[20] made on a thin-film stack with a similar composition to the one used in our experiment, one way to accomplish this task is to irradiate the sample in two steps: (i) the first step of irradiation, called background irradiation, on an area larger than the artificial nucleation center with low ion dose; (ii) the second step of irradiation, with a higher ion dose in a geometry within the background region, to create the artificial nucleation center. Despite the similar film composition with respect to the results presented in ref 20, a different ion dose value is expected to be found in order to obtain the same effect due to the slightly different thickness of the deposited CoFeB and process variations introduced in the sample fabrication. The goal of the irradiation study is to identify the best ion dose to obtain a reliable nucleation in the devices under study.

The aim of the background irradiation is to set up a favorable environment for the nucleation that occurs in the spot with weak PMA. Being the background irradiation characterized by a lower ion dose with respect to the one used in the second irradiation step, it mediates the transition between the weak PMA region (high ion dose) and the pristine region (no irradiation).

In order to get values of the ion doses needed for the two Ga$^+$ irradiations, regions of the continuous thin film were uniformly irradiated with different ion doses to observe the change of the average domain size. The results, after demagnetizing the sample, are shown in Figure 2a. For low ion doses, the size of the domains remains unaltered. From 6.2 × 10^{12} ions/cm^2 the domain size starts to increase up to 9.5 × 10^{12} ions/cm^2, where the domain fills up the entire irradiation square. This last dose is chosen to be the background irradiation dose since the domain size increases reaching the peak. For higher ion doses, the domain size drops again toward values below the optical resolution.

Once the background irradiation dose is defined, the next step is to find the ion dose for which the switching field of an irradiated patterned structure is lowered the most. Irradiating structures locally with this ion dose is then used to create the artificial nucleation centers, i.e., low switching field spots. Patterned microdisks, with diameters ranging from 7 to 10 μm, were first irradiated entirely with the background irradiation dose (9.5 × 10^{12} ions/cm^2) and, second, a square of 500 × 500 nm^2 was irradiated in their center. The motivation for choosing microdisks of different sizes lies in the fact that different lithography test structures were exploited on the same sample. In this way, it is expected that the same ion doses can be used to reproduce the results of the irradiation study of the next experiment involving ferromagnetic wires (see Irradiation Study section). On the other hand, using another sample for the irradiation study could lead to different results due to deposition variations of the sputtering tool.

In order to measure the switching field, 50 field pulses, 5 ms wide, were applied. This train of pulses was then repeated for different positive amplitudes. Between each pulse, a negative

pulse is applied to saturate the disks in the negative magnetization direction. According to this procedure, the magnets are saturated in the negative magnetization direction, and an image is recorded. Then the pulse, to measure the switching field, is applied, and another image is recorded. By subtracting the two images, a differential image is obtained, from which it is possible to detect the magnetic reversal of the disks. Thus, 50 differential images, for each amplitude, are recorded to better estimate the switching field. The results are reported in Figure 2b.

For low ion doses, the switching field drops toward very low values. As soon as the ion dose increases, the switching field increases and saturates to a value of about 9 mT. Assuming that before the irradiation of the nucleation centers the disks are set to their highest switching field, due to the background irradiation, and considering that any further irradiation will cause a reduction of the switching field (according to the average domain size trend, which reflects the switching field trend[20]), the switching field trend of the disks (see Figure 2b) tells us that going toward strong irradiation does not mean that the nucleation process will occur at lower magnetic field values. One possible explanation for the trend can be related to the energy difference between the weak PMA spot and the surrounding area. In particular, a stronger irradiation increases the energy step that the nucleating domain should overcome.

The outcomes of this first part of the study allowed to identify the optimal ion doses to create the artificial nucleation center according to the two-step irradiation: we identified the background dose, around 1×10^{13} ions/cm^2, and the artificial nucleation center dose, around 2.5×10^{13} ions/cm^2 (background dose included).

During the background irradiation analysis, we observed a change of the domain size, which, in turn, corresponds to a change in the material magnetic properties. Taking into account this result, is it possible to create motion barriers able to stop the domain wall motion? Moreover, is it possible to tune the strength of them with FIB irradiation? In order to address these questions, barriers have been irradiated onto microtrack and tested by means of magnetic field and current-driven domain wall motion.

Field-Driven Domain Motion through Irradiated Regions. Although we showed that the artificial nucleation center correctly improves the nucleation process by reducing the switching field and defining the nucleation position, this work is focused on the experimental demonstration of FIB-irradiated regions able to stop a moving domain wall, that could be unpinned with a stimulus above a certain current (or field) threshold. In this way, the driving force of the domain wall can be increased in order to increase the domain wall speed and avoid intrinsic pinning events due to defects present on the track, while allowing to have a control of the shifting of the domain from one barrier to the other. Therefore, a proper tuning of the confinement strength is needed.

The experimental setup used to perform our experiments is schematically represented in Figure 3c. Magnetic field pulses are used to move the domain wall in a 6 μm wide track. In first place, according to the irradiation study, an ANC is placed near the left edge to define the position of the domain wall nucleation. Successively, different barriers are placed along the track by irradiating 500 nm wide perpendicular lines, as shown by the dashed lines in Figure 3c. The distance between each barrier is 50 μm to avoid interaction between each irradiated region. The track is in the pristine state, and only the regions

corresponding to the ANC and to the barriers are irradiated. Each barrier is irradiated with a different ion dose. In particular, starting from the first barrier placed after the ANC on the left, the ion dose is increased from $\approx 5 \times 10^{12}$ ions/cm^2 to $\approx 1 \times 10^{13}$ ions/cm^2 from left to right. Note that the highest ion dose used is close to the background irradiation dose, where the highest average domain size (linked to the highest switching field) is found.

First, a domain is nucleated near the left edge of the track thanks to the ANC. Magnetic field pulses of 3.7 mT of 5 ms are used for the nucleation. Second, magnetic field pulses ranging from 0.5 to 1 mT with a pulse width of 5 ms are applied to expand the nucleated domain. Consequently, the corresponding domain wall moves toward the right, facing the different barriers placed along the track one after the other. After each field pulse, a WMOKE image is recorded and the position of the domain wall is detected. In Figure 4 the
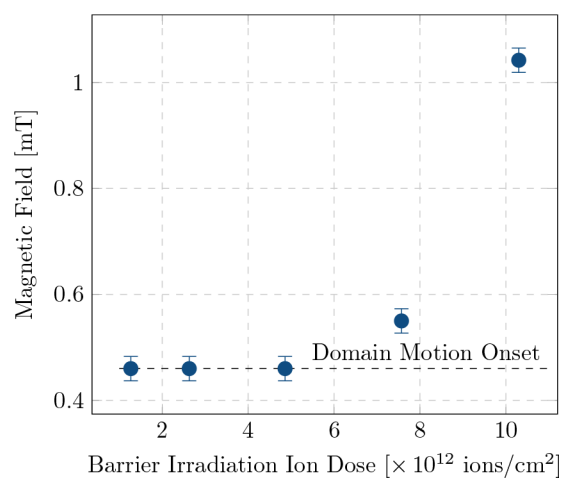

Figure 4. Evolution of the magnetic field needed to make the domain wall overcoming the different Ga$^+$ FIB irradiated barriers shown in Figure 3c.

minimum field needed to overcome the barrier is plotted against the ion dose of the barrier, clearly showing an increase of the barrier strength with the ion doses for the highest irradiation values. In particular, for low ion dose, up to $\approx 4.9 \times 10^{12}$ ions/cm^2, the domain wall motion does not seem to be affected by the barriers. Here we assume that the irradiation does not affect the material parameters enough to produce a visible effect and the magnetic field value recorded corresponds to the one needed to start the motion (depicted by the dashed line in Figure 4). For ion doses higher than $\approx 4.9 \times 10^{12}$, the domain wall motion starts to be obstructed. The obstruction phenomena is registered up to a value of $\approx 1 \times 10^{13}$ where the field required to unpin the domain wall produces a complete reversal of the magnetization of the wire.

Another important characteristic of the phenomenon is related to the domain wall–barrier interaction: when the domain wall enters the irradiated region, it is not able to escape from that region until a certain magnetic field threshold is reached. The domain wall does not move out of the irradiated zone applying the magnetic field in both directions, which means that the domain wall is trapped into the irradiated region. In other words, this means that the irradiated region is an energy well rather than a barrier, which can be counterintuitive considering that up to the background ion
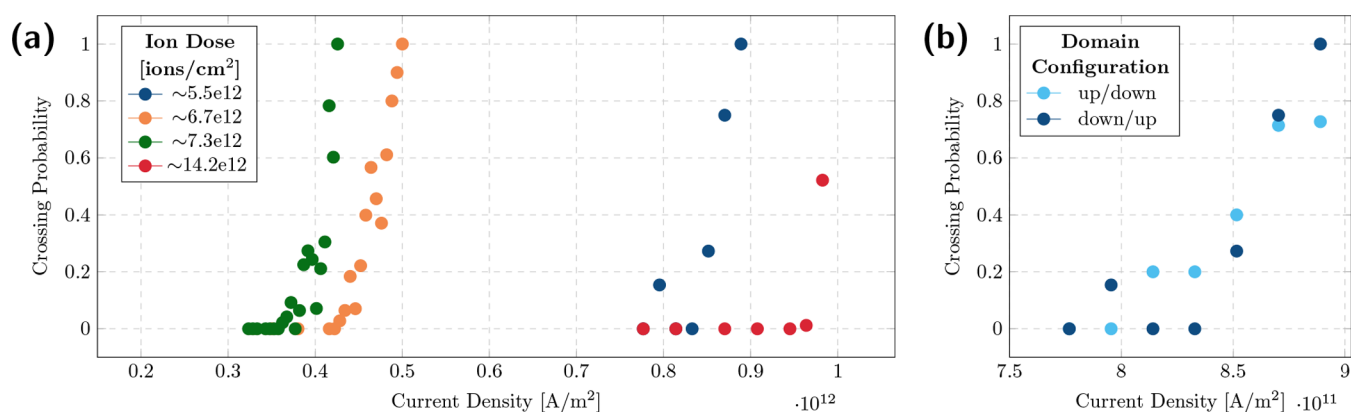
Figure 5. (a) Crossing probability of a domain wall over the applied current density. The curves for barriers with different ion doses are shown in different colors. (b) Probability curves for $\sim 5.5 \times 10^{12}$ ions/cm^2 for different magnetization of the domain wall.

dose ($\sim 1 \times 10^{13}$ ions/cm^2) the switching field increases. In order to better understand how the domain wall behaves in overcoming the step from the irradiated region to the pristine one, micromagnetic simulations were performed. The results are discussed in the Micromagnetic Simulations section.

After investigating the motion of the domain wall through the irradiated regions by means of magnetic field pulses, the next experiment involves the use of current pulses to move the domain wall.

Current-Induced Domain Wall Motion through Irradiated Regions. In this section, we explore the behavior of the domain wall motion through irradiated regions by using current pulses injected into the ferromagnetic wire. The use of the current pulses carries many advantages with respect to magnetic field pulses, such as the possibility to easily integrate ferromagnetic tracks into electronic circuits and the possibility to easily access the nanosecond regime.

Figure 3b shows the irradiation scheme on the ferromagnetic tracks used for the experiment. The artificial nucleation center is placed on the left-hand side of the track, ensuring the nucleation position. Once nucleated, the domain wall propagates toward the right as dictated by the current direction. Its motion is then stopped by the barrier placed on the right-hand side of the track. From this configuration, the measurement starts, which consists of the injection of 100 current pulses into the ferromagnetic track with a duration of 100 ns each. After each pulse, an image is recorded to verify the position of the domain wall. After one train of pulses, the pulse's amplitude is increased and the measurement is repeated. The different measurements are then postprocessed, and the detection of the crossing of the domain wall is analyzed by subtracting each image with respect to the initial image, corresponding to the initial position of the domain wall. In this way, the relative displacement of the domain wall can be detected and the probability, over 100 pulses, of the domain wall to cross the barrier is calculated for each current amplitude. The same set of measurements is then repeated for different ferromagnetic tracks having barriers with different ion doses. According to this procedure, probability curves for each ion doses used are built.

The results are shown in Figure 5. In the first place, changing the ion dose used to irradiate the barrier region, the probability curves are clearly shifted. It means that the strength of the barrier is influenced by the irradiation ion dose. For the ion dose of $\approx 5.5 \times 10^{12}$ ions/cm^2 the current density needed

to overcome the barrier is around 8.5×10^{11} A/m^2. As the ion dose increases, as for the green and orange dots, the required current density is lowered. In particular, for the ion dose of $\approx 7.3 \times 10^{12}$ ions/cm^2 the current density is halved. Increasing further the ion dose, as for the case of $\approx 1.42 \times 10^{13}$ ions/cm^2 (red points), the domain wall crosses the barrier for higher current density, even higher than the case of lowest ion dose (blue dots). It is worth to notice that the red points do not reach the probably equal to one. This is due to the high current density used, which damages the track due to Joule heating for the pulse width employed. Summarizing the results, for low ion doses, the current density needed to overcome the pinning site decreases as the ion dose increases. In this range, the irradiation lowers the strength of the barrier. For high ion doses, the current density increases, meaning that the pinning strength increases. The reasons for this unexpected behavior are discussed in the next section, where micromagnetic simulations were performed to support the discussion.

Figure 5b shows two probability curves which are built by measuring the same barrier (with ion dose equal to $\approx 5.5 \times 10^{12}$ ions/cm^2) but changing the domain wall magnetization. In particular, the cyan dots depict measurements considering an up−down domain wall, while the blue ones illustrate measurements with a down−up domain wall. As can be observed, within the range of the measurement accuracy, we see the same behavior for an up/down as for a down/up domain wall, as expected. The results show the absence of a magnetic field supporting the expansion of a particular domain direction and the correctness of the performed measurements.

The analysis shows clearly that it is possible to tune the barrier strength by setting the FIB ion dose. From the application point of view, it is possible to create regions in which domains can be confined.

To better understand the behavior and the motion of the domain wall through the irradiated regions, we performed micromagnetic simulations, whose results are discussed below.

Micromagnetic Simulations. Micromagnetic simulations are used to study the effects of the irradiation in the barrier region. The simulation domain involves a 1024×512 nm^2 micro track, in which the left half represents the FIB irradiated region. In this region the saturation magnetization and the uniaxial anisotropy values are modified to replicate the irradiation effects, while in the right half of the track the material parameters are kept at the pristine values (reported in Table 1. The parameters, presented in Table 1, for the pristine
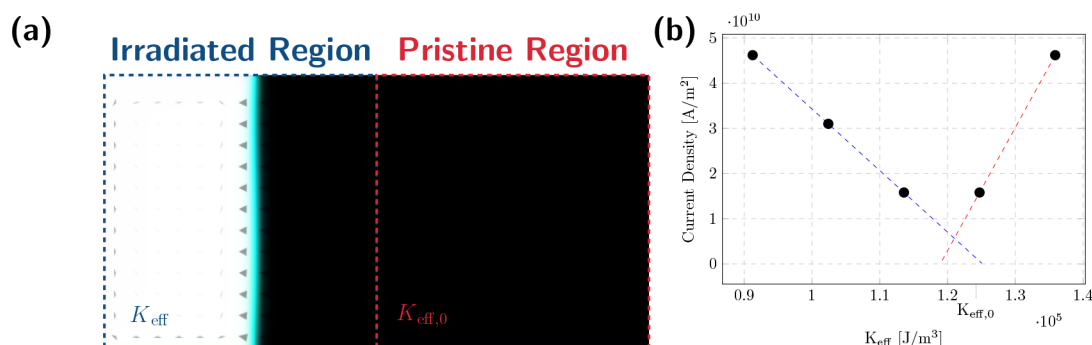
Figure 6. Micromagnetic simulations of domain wall motions through a K_{eff} step. (a) Simulation frame of a domain wall initialized into the left-hand half of the track. In this region, representing the irradiated region, K_{eff} is varied with respect to the value in the pristine region ($K_{eff,0}$), represented by the right-hand half of the track. A spin-Hall effect current generates a spin-polarized current flowing toward the right, causing the motion of the domain wall. (b) Evolution of the current density needed to overcome the K_{eff} step between the irradiated and the pristine regions.

part of the track are taken from previous works,[20] involving the same stack. A domain wall is initialized in the left half of the track, where the effective magnetic anisotropy K_{eff} is varied. In the simulations, no periodic boundary conditions are applied. This is done because, since the magnetization on the left boundary is opposite to the one on the right side, the simulation domain cannot be replicated along the longitudinal direction of the track. Moreover, because the magnetization tilts at the edges of the track due to the presence of DMI, the domain wall is initialized far enough from the left edge, avoiding the interaction between the edge and the domain wall. After an initial relax of the system, to reach an equilibrium configuration, a SOT current is injected for 10 ns, resulting in the motion of the domain wall to the right. The moving domain wall then faces a step in K_{eff} in the middle of the track, as shown in Figure 6a. The height of the step is determined by the difference between K_{eff}, the effective magnetic anisotropy of the left-hand side of the track, and the one in the pristine region $K_{eff,0}$. On the left-hand side of the track, K_{eff} is varied by changing the K_u value between different simulations, while M_S is kept constant. The simulation is performed for different values of K_{eff} and SOT current. In each simulation the current density needed to overcome the step, the depinning current, is recorded. The results of the simulations are highlighted in Figure 6b. Here, two trends can be identified: increasing K_{eff}, starting from the lowest value, the current needed to overcome the step decreases linearly (blue curve). This is related to the change of the K_{eff} step height. In particular, increasing K_{eff}, the step height decreases because we are getting closer to the value in the pristine region ($K_{eff,0}$). This means that once the domain encounters the step, the torque applied by the SOT current needed to overcome the step is lower as K_{eff} increases. For higher values of K_{eff}, the depinning current increases again (red curve). This last increase can be mainly related to the change in the magnetic properties of the region in which the domain wall is initialized. In particular, the values of K_{eff} in this regime are higher than $K_{eff,0}$, which means that the system becomes more rigid and the domain wall requires higher torque to move. Assuming that in this regime, the increasing in the depinning current is not related to the difference between $K_{eff,0}$ and K_{eff}, but it can be related to an increasing of the current needed to provide the higher torque.

Experimentally, from the background irradiation study, we observed an increase of the average domain size, which can be related to an increase of the effective magnetic anisotropy. For irradiation doses higher than the background irradiation dose,

the average domain size decreases, corresponding to a decreasing of K_{eff}. Comparing the experimental results on the current-induced domain-wall motion (in which the depinning current is observed to initially decrease and then to increase) with the simulation results mentioned above, some hypothesis to match the behavior in both experiment and simulation can be proposed: let us consider the pristine value of K_{eff} to lie on the blue curve. In this case, irradiating with ion doses below the background irradiation dose, we are moving from the blue curve toward the red one. In this way, the depinning current initially decreases to then increase again when the K_{eff} values fall into the red curve. This hypothesis would explain the experimental behavior; however, it assumes a monotonic increase of K_{eff}. Instead, if we assume to start from a point on the blue curve, and considering an increase of K_{eff} followed by a decrease, the experiment matches the simulation considering a point moving along the blue curve toward the red one, but to climb back to the blue curve before entering the regime depicted by the red curve. According to this hypothesis, during the increase of K_{eff} due to ion doses below the background irradiation, the depinning current decreases, while it increases again due to the decrease of K_{eff} for ion doses higher than the background irradiation dose.

From the simulations, it is clear that the current needed to overcome a step in the effective magnetic anisotropy can be finely tuned depending on the reduction of K_{eff}. This allows us to design and tune an artificial pinning site on the track, which is required to schematically shift a domain.

CONCLUSIONS

In this paper, we demonstrated how Ga^+ irradiation can be used to create artificial nucleation centers and, more importantly, to define and tune the strength of artificial pinning sites. First, a preliminary study was performed to identify the proper ion dose to create ANC required to nucleate domains. Second, FIB-irradiated barriers, perpendicular to the tracks, were created to introduce artificial pinning sites. Results showed that the pinning strength of such barriers can be tuned by controlling the Ga^+ irradiation dose. Field-driven domain wall motion showed a proportional relation between the field required to overcome the barrier and its strength. For the current-driven experiments, the current density needed to push the domain over the pinning sites decreases for increasing ion doses up to $\approx 7.3 \times 10^{12}$ ions/cm². For higher ion doses, the required current density increases again. Supportive micromagnetic simulations have been

performed to better understand the current-driven motion case. The motion toward a step in effective anisotropy was studied. Results showed two regimes on K_{eff}: for K_{eff} values smaller than the pristine value, the current density needed to overcome the step increases as K_{eff} decreases. On the other hand, for K_{eff} values larger than the pristine value, the required current density increases for increasing values of K_{eff} due to the higher torque needed to initiate the domain wall motion. Further studies are needed to understand the impact of the irradiation on other material parameters, such as DMI, damping. These findings show that Ga^+ ion irradiation can be a powerful tool to tune the material properties, for both defining ANCs and defining artificial pinning sites of different strengths depending on the ion dose employed. The possibility to finely tune the strength of the pinning site could ease the application of this technology in-memory applications, for a rigid and controlled domain-wall shift, or for neuromorphic computation, where different weights can be defined into the FIB-irradiated pinning sites.

■ AUTHOR INFORMATION

Corresponding Author

Fabrizio Riente − *Department of Electronics and Telecommunications, Politecnico di Torino, 10129 Torino, Italy;* ⊙ orcid.org/0000-0003-4147-1098;
Email: fabrizio.riente@polito.it

Authors

Domenico Giuliano − *Department of Electronics and Telecommunications, Politecnico di Torino, 10129 Torino, Italy*

Luca Gnoli − *Department of Electronics and Telecommunications, Politecnico di Torino, 10129 Torino, Italy*

Valentin Ahrens − *Nanomagnetic Devices Group, Chair of Nano and Quantum Sensors, Department of Electrical and Computer Engineering, Technical University of Munich, Munich 80333, Germany*

Massimo Ruo Roch − *Department of Electronics and Telecommunications, Politecnico di Torino, 10129 Torino, Italy*

Markus Becherer − *Nanomagnetic Devices Group, Chair of Nano and Quantum Sensors, Department of Electrical and Computer Engineering, Technical University of Munich, Munich 80333, Germany*

Giovanna Turvani − *Department of Electronics and Telecommunications, Politecnico di Torino, 10129 Torino, Italy*

Marco Vacca − *Department of Electronics and Telecommunications, Politecnico di Torino, 10129 Torino, Italy*

Complete contact information is available at:
https://pubs.acs.org/10.1021/acsaelm.2c01510

Notes

The authors declare no competing financial interest.

■ REFERENCES

(1) Dieny, B.; Prejbeanu, I. L.; Garello, K.; Gambardella, P.; Freitas, P.; Lehndorff, R.; Raberg, W.; Ebels, U.; Demokritov, S. O.; Akerman, J.; et al. Opportunities and challenges for spintronics in the microelectronics industry. *Nat. Electron.* **2020**, *3*, 446−459.

(2) Raymenants, E.; Wan, D.; Couet, S.; Canvel, Y.; Thiam, A.; Tsvetanova, D.; Souriau, L.; Asselberghs, I.; Carpenter, R.; Jossart, N.; et al.*Magnetic Domain Walls: From Physics to Devices*; 2021 IEEE International Electron Devices Meeting (IEDM); 2021; pp 32−3.

(3) Raymenants, E.; Bultynck, O.; Wan, D.; Devolder, T.; Garello, K.; Souriau, L.; Thiam, A.; Tsvetanova, D.; Canvel, Y.; Nikonov, D. E.; Young, I. A.; Heyns, M.; Soree, B.; Asselberghs, I.; Radu, I.; Couet, S.; Nguyen, V. D. Nanoscale domain wall devices with magnetic tunnel junction read and write. *Nat. Electron.* **2021**, *4*, 392−398.

(4) Kumar, D.; Jin, T.; Sbiaa, R.; Kläui, M.; Bedanta, S.; Fukami, S.; Ravelosona, D.; Yang, S.-H.; Liu, X.; Piramanayagam, S. Domain wall memory: Physics, materials, and devices. *Phys. Rep.* **2022**, *958*, 1−35.

(5) Luo, Z.; Hrabec, A.; Dao, T. P.; Sala, G.; Finizio, S.; Feng, J.; Mayr, S.; Raabe, J.; Gambardella, P.; Heyderman, L. J. Current-driven magnetic domain-wall logic. *Nature* **2020**, *579*, 214−218.

(6) Parkin, S. S.; Hayashi, M.; Thomas, L. Magnetic domain-wall racetrack memory. *Science* **2008**, *320*, 190−194.

(7) Allwood, D. A.; Xiong, G.; Faulkner, C.; Atkinson, D.; Petit, D.; Cowburn, R. Magnetic domain-wall logic. *science* **2005**, *309*, 1688−1692.

(8) Burrowes, C.; Vernier, N.; Adam, J.-P.; Herrera Diez, L.; Garcia, K.; Barisic, I.; Agnus, G.; Eimer, S.; Kim, J.-V.; Devolder, T.; Lamperti, A.; Mantovan, R.; Ockert, B.; Fullerton, E. E.; Ravelosona, D. Low depinning fields in Ta-CoFeB-MgO ultrathin films with perpendicular magnetic anisotropy. *Appl. Phys. Lett.* **2013**, *103*, 182401.

(9) Manchon, A.; Železný, J.; Miron, I. M.; Jungwirth, T.; Sinova, J.; Thiaville, A.; Garello, K.; Gambardella, P. Current-induced spin-orbit torques in ferromagnetic and antiferromagnetic systems. *Rev. Mod. Phys.* **2019**, *91*, 035004.

(10) Manchon, A.; Železný, J.; Miron, I. M.; Jungwirth, T.; Sinova, J.; Thiaville, A.; Garello, K.; Gambardella, P. Current-induced spin-orbit torques in ferromagnetic and antiferromagnetic systems. *Rev. Mod. Phys.* **2019**, *91*, 035004.

(11) Hoffmann, A. Spin Hall effects in metals. *IEEE Trans. Magn.* **2013**, *49*, 5172−5193.

(12) Bläsing, R.; Khan, A. A.; Filippou, P. C.; Garg, C.; Hameed, F.; Castrillon, J.; Parkin, S. S. Magnetic racetrack memory: From physics to the cusp of applications within a decade. *Proceedings of the IEEE* **2020**, *108*, 1303−1321.

(13) Atkinson, D.; Allwood, D. A.; Xiong, G.; Cooke, M. D.; Faulkner, C. C.; Cowburn, R. P. Magnetic domain-wall dynamics in a submicrometre ferromagnetic structure. *Nat. Mater.* **2003**, *2*, 85−87.

(14) Devolder, T.; Barisic, I.; Eimer, S.; Garcia, K.; Adam, J.-P.; Ockert, B.; Ravelosona, D. Irradiation-induced tailoring of the magnetism of CoFeB/MgO ultrathin films. *Journal of applied Physics* **2013**, *113*, 203912.

(15) Herrera Diez, L.; Garcia-Sanchez, F.; Adam, J.-P.; Devolder, T.; Eimer, S.; El Hadri, M.; Lamperti, A.; Mantovan, R.; Ocker, B.; Ravelosona, D. Controlling magnetic domain wall motion in the creep regime in He+-irradiated CoFeB/MgO films with perpendicular anisotropy. *Appl. Phys. Lett.* **2015**, *107*, 032401.

(16) Franken, J.; Hoeijmakers, M.; Lavrijsen, R.; Kohlhepp, J.; Swagten, H.; Koopmans, B.; Van Veldhoven, E.; Maas, D. Precise control of domain wall injection and pinning using helium and gallium focused ion beams. *J. Appl. Phys.* **2011**, *109*, 07D504.

(17) Franken, J. H.; Hoeijmakers, M.; Lavrijsen, R.; Swagten, H. J. Domain-wall pinning by local control of anisotropy in Pt/Co/Pt strips. *J. Phys.: Condens. Matter* **2012**, *24*, 024216.

(18) Ahrens, V.; Gnoli, L.; Giuliano, D.; Mendisch, S.; Kiechle, M.; Riente, F.; Becherer, M. Skyrmion velocities in FIB irradiated W/CoFeB/MgO thin films. *AIP Adv.* **2022**, *12*, 035325.

(19) Ahrens, V.; Kiesselbach, C.; Gnoli, L.; Giuliano, D.; Mendisch, S.; Kiechle, M.; Riente, F.; Becherer, M. Skyrmions Under Control−

FIB Irradiation as a Versatile Tool for Skyrmion Circuits. *Adv. Mater.* **2022**, 2207321.

(20) Mendisch, S.; Riente, F.; Ahrens, V.; Gnoli, L.; Haider, M.; Opel, M.; Kiechle, M.; Roch, M. R.; Becherer, M.Controlling Domain-Wall Nucleation in Ta/CoFeB/MgO Nanomagnets via Local Ga+ Ion Irradiation. *arXiv preprint arXiv:2102.07540*, 2021.

(21) Juge, R.; Bairagi, K.; Rana, K. G.; Vogel, J.; Sall, M.; Mailly, D.; Pham, V. T.; Zhang, Q.; Sisodia, N.; Foerster, M.; Aballe, L.; Belmeguenai, M.; Roussigné, Y.; Auffret, S.; Buda-Prejbeanu, L. D.; Gaudin, G.; Ravelosona, D.; Boulle, O. Helium Ions Put Magnetic Skyrmions on the Track. *Nano Lett.* **2021**, *21*, 2989−2996.

(22) Franken, J.; Swagten, H.; Koopmans, B. Shift registers based on magnetic domain wall ratchets with perpendicular anisotropy. *Nat. Nanotechnol.* **2012**, *7*, 499−503.

(23) Franken, J. H.; van der Heijden, M. A.; Ellis, T. H.; Lavrijsen, R.; Daniels, C.; McGrouther, D.; Swagten, H. J.; Koopmans, B. Beam-Induced Fe Nanopillars as Tunable Domain-Wall Pinning Sites. *Adv. Funct. Mater.* **2014**, *24*, 3508−3514.

(24) Riente, F.; Ziemys, G.; Mattersdorfer, C.; Boche, S.; Turvani, G.; Raberg, W.; Luber, S.; Gamm, S. B. Controlled data storage for non-volatile memory cells embedded in nano magnetic logic. *AIP Adv.* **2017**, *7*, 055910.

(25) Vansteenkiste, A.; Leliaert, J.; Dvornik, M.; Helsen, M.; Garcia-Sanchez, F.; Van Waeyenberge, B. The design and verification of MuMax3. *AIP advances* **2014**, *4*, 107133.

(26) Tomasello, R.; Martinez, E.; Zivieri, R.; Torres, L.; Carpentieri, M.; Finocchio, G. A strategy for the design of skyrmion racetrack memories. *Sci. Rep.* **2014**, *4*, 1−7.

(27) Zhao, X.; Zhang, B.; Vernier, N.; Zhang, X.; Sall, M.; Xing, T.; Diez, L. H.; Hepburn, C.; Wang, L.; Durin, G.; Casiraghi, A.; Belmeguenai, M.; Roussigné, Y.; Stashkevich, A.; Chérif, S. M.; Langer, J.; Ocker, B.; Jaiswal, S.; Jakob, G.; Kläui, M.; Zhao, W.; Ravelosona, D. Enhancing domain wall velocity through interface intermixing in W-CoFeB-MgO films with perpendicular anisotropy. *Appl. Phys. Lett.* **2019**, *115*, 122404.

(28) Diez, L. H.; Voto, M.; Casiraghi, A.; Belmeguenai, M.; Roussigné, Y.; Durin, G.; Lamperti, A.; Mantovan, R.; Sluka, V.; Jeudy, V.; et al. Enhancement of the Dzyaloshinskii-Moriya interaction and domain wall velocity through interface intermixing in Ta/CoFeB/MgO. *Phys. Rev. B* **2019**, *99*, 054431.